Self-referenced characterization of femtosecond laser pulses by chirp scan

Vincent Loriot,[1,*] Gregory Gitzinger,[2] and Nicolas Forget[2]

[1] *Institut Lumière Matière, UMR5306 Université Lyon 1-CNRS, Université de Lyon 69622 Villeurbanne cedex, France*

[2] *FASTLITE, Les Collines de Sophia Bât. D1, 1900 route des Crêtes, 06560 Valbonne, France*

[*] *vincent.loriot@univ-lyon1.fr*

Abstract: We investigate a variant of the d-scan technique, an intuitive pulse characterization method for retrieving the spectral phase of ultrashort laser pulses. In this variant a ramp of quadratic spectral phases is applied to the input pulses and the second harmonic spectra of the resulting pulses are measured for each chirp value. We demonstrate that a given field envelope produces a unique and unequivocal chirp-scan map and that, under some asymptotic assumptions, both the spectral amplitude and phase of the measured pulse can be retrieved analytically from only two measurements. An iterative algorithm can exploit the redundancy of the information contained in the chirp-scan map to discard experimental noise, artifacts, calibration errors and improve the reconstruction of both the spectral intensity and phase. This technique is compared to two reference characterization techniques (FROG and SRSI). Finally, we perform d-scan measurements with a simple grating-pair compressor.

OCIS codes: (320.7100) Ultrafast measurements; (320.5540) Pulse shaping.

References and links

1. I. A. Walmsley and C. Dorrer, "Characterization of ultrashort electromagnetic pulses," Adv. Opt. Photon. **1**, 308–437 (2009).
2. P. O'shea, M. Kimmel, X. Gu, and R. Trebino, "Highly simplified device for ultrashort-pulse measurement," Opt. Lett. **26**, 932–934 (2001).
3. A. S. Radunsky, I. A. Walmsley, S.-P. Gorza, and P. Wasylczyk, "Compact spectral shearing interferometer for ultrashort pulse characterization," Opt. Lett. **32**, 181–183 (2007).
4. R. Trebino, K. W. DeLong, D. N. Fittinghoff, J. N. Sweetser, M. A. Krumbugel, B. A. Richman, and D. J. Kane, "Measuring ultrashort laser pulses in the time-frequency domain using frequency-resolved optical gating," Rev. Sci. Instrum. **68**, 3277–3295 (1997).
5. C. Iaconis and I. Walmsley, "Spectral phase interferometry for direct electric-field reconstruction of ultrashort optical pulses," Opt. Lett. **23**, 792–794 (1998).
6. V. V. Lozovoy, I. Pastirk, and M. Dantus, "Multiphoton intrapulse interference. iv. ultrashort laser pulse spectral phase characterization and compensation," Opt. Lett. **29**, 775–777 (2004).
7. V. V. Lozovoy, B. Xu, Y. Coello, and M. Dantus, "Direct measurement of spectral phase for ultrashort laser pulses," Opt. Express **16**, 592–597 (2008).
8. B. Xu, J. M. Gunn, J. M. D. Cruz, V. V. Lozovoy, and M. Dantus, "Quantitative investigation of the multiphoton intrapulse interference phase scan method for simultaneous phase measurement and compensation of femtosecond laser pulses," J. Opt. Soc. Am. B **23**, 750–759 (2006).
9. S. Grabielle, N. Forget, S. Coudreau, T. Oksenhendler, D. Kaplan, J.-F. Hergott, and O. Gobert, "Local spectral compression method for cpa lasers," in "CLEO Europe-EQEC 2009" (IEEE, 2009).
10. S. Grabielle, "Manipulation et caractrisation du champ lectrique optique: applications aux impulsions femtosecondes," Ph.D. thesis, Ecole Polytechnique (2011).

#195491 - $15.00 USD Received 8 Aug 2013; revised 26 Sep 2013; accepted 26 Sep 2013; published 10 Oct 2013

11. "Application note 38 - automated control of amplitied pulse duration using the dazzler/dazcope solution," Tech. rep., Newport Corporation (2009).
12. M. Miranda, T. Fordell, C. Arnold, A. L'Huillier, and H. Crespo, "Simultaneous compression and characterization of ultrashort laser pulses using chirped mirrors and glass wedges," Opt. Express **20**, 688 (2012).
13. M. Miranda, C. L. Arnold, T. Fordell, F. Silva, B. Alonso, R. Weigand, A. L'Huillier, and H. Crespo, "Characterization of broadband few-cycle laser pulses with the d-scan technique," Opt. Express **20**, 18732–18743 (2012).
14. M. Miranda, P. Rudawski, C. Guo, F. Silva, C. L. Arnold, T. Binhammer, H. Crespo, and A. L'Huillier, "Ultrashort laser pulse characterization from dispersion scans: a comparison with spider," in "CLEO: QELS_Fundamental Science," (OSA, 2013).
15. I. Pastirk, B. Resan, A. Fry, J. MacKay, and M. Dantus, "No loss spectral phase correction and arbitrary phase shaping of regeneratively amplified femtosecond pulses using miips," Opt. Express **14**, 9537–9543 (2006).
16. N. Forget, V. Crozatier, and T. Oksenhendler, "Pulse-measurement techniques using a single amplitude and phase spectral shaper," J. Opt. Soc. Am. B **27**, 742–756 (2010).
17. S. Grabielle, A. Moulet, N. Forget, V. Crozatier, S. Coudreau, R. Herzog, T. Oksenhendler, C. Cornaggia, and O. Gobert, "Self-referenced spectral interferometry cross-checked with spider on sub-15fs pulses," Nucl. Instrum. Methods Phys. Res., Sect. A **653**, 121–125 (2011).
18. G. Taft, A. Rundquist, M. M. Murnane, I. P. Christov, H. C. Kapteyn, K. W. DeLong, D. N. Fittinghoff, M. Krumbugel, J. N. Sweetser, and R. Trebino, "Measurement of 10-fs laser pulses," IEEE J. Quantum Electron. **2**, 575–585 (1996).
19. A. Baltuska, M. S. Pshenichnikov, and D. A. Wiersma, "Amplitude and phase characterization of 4.5-fs pulses by frequency-resolved optical gating." Opt. Lett. **23**, 1474–1476 (1998).
20. S. Akhmanov, A. Chirkin, K. Drabovich, A. Kovrigin, R. Khokhlov, and A. Sukhorukov, "Nonstationary nonlinear optical effects and ultrashort light pulse formation," IEEE J. Quantum Electron., **4**, 598–605 (1968).
21. E. Chassande-mottin and P. Flandrin, "On the time-frequency detection of chirps," Appl. Comput. Harmon. Anal. **281**, 252–281 (1999).
22. P. Tournois, "Acousto-optic programmable dispersive filter for adaptive compensation of group delay time dispersion in laser systems," Opt. Commun. **140**, 245–249 (1997).
23. T. Oksenhendler, S. Coudreau, N. Forget, V. Crozatier, S. Grabielle, R. Herzog, O. Gobert, and D. Kaplan, "Self-referenced spectral interferometry," Appl. Phys. B **99**, 7–12 (2010).
24. A. Moulet, S. Grabielle, C. Cornaggia, N. Forget, and T. Oksenhendler, "Single-shot, high-dynamic-range measurement of sub-15 fs pulses by self-referenced spectral interferometry," Opt. Lett. **35**, 3856–3858 (2010).

Ultrashort pulse metrology has been a rapidly advancing field of research for more than three decades [1]. The development of optical femtosecond sources with record pulse durations, peak intensities, pulse contrast, tunability or pulse complexity has been constantly rising new challenges and triggered the search for new pulse characterization techniques. Parallel to the deployment of ever more sophisticated and specialized techniques, substantial efforts were made to simplify setups and provide compact, intuitive and quantitative pulse diagnostics. Techniques such as GRENOUILLE [2] or ARAIGNEE [3] are examples of successful attempts to scale down and simplify the experimental setups of SH-FROG [4] and SPIDER [5].

More recently, measurement methods such as MIIPS [6–8], variant of MIIPS [9–11] and dispersion scan (d-scan) [12–14] have emerged. Both MIIPS and d-scan are scanning techniques belonging to the class of phase-only techniques: a set of test spectral phase functions is applied to an unknown electric field $E(t)$ and for each test phase the second harmonic spectrum is recorded. The test functions are usually parameterized by a single scalar parameter p and the experimental data take the form of a two-dimensional map $I_{\mathrm{SHG}}(\omega, p)$. For MIIPS in its original version [6, 8], the test phase functions are sinusoidal functions with a period depending on the spectral bandwidth and where the parameter p is a phase offset. For d-scan and some variants of MIIPS [7], the test phases are polynomial functions and the parameter is a dispersion coefficient. An iterative algorithm then retrieves the spectral phase (d-scan) or an approximation of the spectral phase (MIIPS).

In spite of their scanning nature, MIIPS and d-scan roused a significant interest owing to the simplicity of the experimental setup (minimal alignment, single-beam geometry without any beam splitting nor beam recombination), its robustness (no assumption on the beam profile, no interferometric stability), and ease of operation. Finally, these techniques can be directly em-

#195491 - $15.00 USD Received 8 Aug 2013; revised 26 Sep 2013; accepted 26 Sep 2013; published 10 Oct 2013

bodied in chirped-pulse amplification systems [15] and used to measure and compress amplified pulses with the same device.

However, from the point of view of optical metrology, several questions remain unanswered. The first opened topic is related to the uniqueness of the retrieved phase. Secondly, these techniques retrieve the spectral phase but do not retrieve the spectral amplitude and require an independent spectrum measurement. The third set of questions concerns the spectral resolution and dynamic range of the measurement. Such questions have been previously addressed for the FROG and the SPIDER and are of major interest to provide a head-to-head comparison with these well-established techniques.

In this paper we theoretically and experimentally investigate a variant of the d-scan technique in which the test functions are pure quadratic phases (chirp-scan). We restrict our study to pulse durations longer than $\simeq$10-15 fs. Within this framework, we demonstrate in sections 1 and 2 that: (i) there is a one-to-one relationship between E(t) and $I_{\mathrm{SHG}}(\omega,\phi_2)$ where ϕ_2 is the chirp coefficient, (ii) $E(t)$ can be analytically retrieved from only two SH measurements if the accessible range of ϕ_2 values is large enough, (iii) $E(t)$ can alternatively be retrieved by an iterative algorithm. In section 3 we demonstrate and compare two pulse retrieval algorithms (CRT and 2D-fit). In section 4 we compare d-scan measurements with two well-established reference techniques (bFROG [16] and SRSI [17]). In section 5, we show how a regular grating-based compressor can be used to perform a d-scan measurement.

1. Second harmonic of chirped pulses

1.1. Second harmonic spectrum

The complex spectral amplitude of the second harmonic (SH) of an optical pulse can be written as the auto-convolution of the complex spectral amplitude of the fundamental pulse. If $E(\omega)$ stands for the complex spectral amplitude of the input pulse the SH signal collected at the angular frequency 2ω can be written as

$$I_{\mathrm{SHG}}(2\omega) \propto \left| \int_{\mathbb{R}} E(\omega-\Omega)E(\omega+\Omega)d\Omega \right|^2 . \tag{1}$$

This simple model of SH generation assumes no absorption, an instantaneous nonlinearity, negligible higher-order nonlinear effects, a thin nonlinear medium and a perfect phase-matching over the bandwidth of interest. With broadband pulses the latter assumption is seldom fulfilled and a more appropriate expression for the SH power spectrum can be derived by including the wavevector-mismatch and other frequency-dependent parameters of the SH and detection stages by adding a spectral filter $R(2\omega)$ [18, 19]. For the sake of clarity, we will however omit $R(2\omega)$ in the following sections.

Equation (1) cannot be simplified without any further assumptions. However, it is well known that the main contributing terms in integrals of the kind $\int_{\mathbb{R}} a(x)\exp[i\phi(x)]\,dx$, where $a(x) > 0$ and $\phi(x)$ are real valued functions, originate from stationary points, i.e. from the vicinity of values x such that $\phi'(x) = 0$. For the SH spectrum, the relevant amplitude and phase functions a and ϕ to be considered are, respectively, $a(\Omega) = |E(\omega-\Omega)E(\omega+\Omega)|$ and $\phi(\Omega) = \arg[E(\omega-\Omega)E(\omega+\Omega)]$. If $E(\omega) = |E(\omega)|\exp[i\varphi(\omega)]$, then the usual stationary phase approximation states that $I_{\mathrm{SHG}}(2\omega)$ reaches a maximum at angular frequencies fulfilling $\varphi'(\omega+\Omega)-\varphi'(\omega-\Omega) \simeq 0$. In particular, this condition is locally fulfilled if $\varphi''(\omega) = 0$. Consequently, the SH spectrum is expected to exhibit a local or global maximum at 2ω if $\varphi''(\omega)$ cancels.

#195491 - $15.00 USD Received 8 Aug 2013; revised 26 Sep 2013; accepted 26 Sep 2013; published 10 Oct 2013

1.2. Quadratic test functions

We now assume that a pure quadratic phase is added before the non linear stage so that the spectral phase of the pulse exciting the non linear process is $\varphi(\omega)+\phi_2(\omega-\omega_0)^2/2$. The measured SH spectrum then becomes:

$$I_{\mathrm{SHG}}(2\omega,\phi_2) \propto \left| \int_{\mathbb{R}} E(\omega-\Omega)E(\omega+\Omega)e^{i\phi_2\Omega^2}d\Omega \right|^2. \tag{2}$$

Equation (2) can be equivalently expressed using the Fourier-transform operator FT:

$$I_{\mathrm{SHG}}(2\omega,\phi_2) \propto \left| FT\left[E^2(t)e^{-it^2/(2\phi_2)}dt\right](2\omega)\right|^2, \tag{3}$$

$I_{\mathrm{SHG}}(2\omega,\phi_2)$ can be seen to be proportional to the square modulus of the Fresnel transform of $E^2(t)$. The analogy between wave propagation and spatial focusing, on one side, and dispersion and temporal focusing on the other side was pointed out as earlier as 1968 [20] and has been a fruitful tool for the understanding and development of temporal characterization methods. From this point of view, performing a chirp-scan measurement by varying ϕ_2 is equivalent to recording the spatial profile at several locations along the beam propagation direction. However, this analogy is not exact since Eq. (3) involves the square of the electric field amplitude instead of the field amplitude itself. Nevertheless, some key features remain valid and this analogy will be used later in this paper. In particular, small and large $|\phi_2|$ values can be associated to respectively near-field and far-field regimes.

1.3. Far-field approximation

Equation (1) can be simplified in the far-field regime, i.e. for large $|\phi_2|$ values. Indeed the integral $\int_{\mathbb{R}} a(x)\exp[i\phi(x)]\,dx$ admits a remarkable asymptotic approximation if $\phi(x)$ exhibits a single and well-defined non degenerate stationary point (i.e. $\phi'(x_0)=0$ and $\phi''(x_0)\neq 0$) [21]:

$$\int_{\mathbb{R}} a(x)e^{i\phi(x)/h}dx \approx_{h\to 0} \sqrt{2\pi}\frac{a(x_0)e^{i\phi(x_0)/h\pm i\frac{\pi}{4}}}{\sqrt{|\phi''(x_0)/h|}} + O\left(h^{\frac{3}{2}}\right), \tag{4}$$

where h is a scaling factor used to express the condition that $\phi'(x)$ takes small values in a very narrow range around x_0. In practice, h is a mute factor and can be ignored. If ϕ possesses a finite number of non degenerate stationary points, the integral can be approximated by the sum of the individual contributions. Besides, the residual error $O\left(h^{\frac{3}{2}}\right)$ has an analytical upper bound which is a function of $a(x)$ and of the higher derivatives of $\phi''(x)$ [21].

Considering the right hand side of Eq. (2), we find that for sufficiently large values of $|\phi_2|$, the overall spectral phase is such that the corresponding group delay is strictly monotonic with frequency and there is a single non-degenerate stationary point for ϕ. The asymptotic expression of the SH spectrum is simply

$$I_{\mathrm{SHG}}(\phi_2,2\omega) \propto \frac{I(\omega)^2}{|\phi_2+\varphi''(\omega)|}. \tag{5}$$

As can be noted, the SH signal tends to diverge when $\phi_2 \simeq -\varphi''(\omega)$. In this particular case, the stationary point becomes degenerate and Eq. (4) is not valid anymore. In practice, the harmonic signal tends to reach a local maximum.

#195491 - $15.00 USD Received 8 Aug 2013; revised 26 Sep 2013; accepted 26 Sep 2013; published 10 Oct 2013

1.4. Uniqueness

For a given wavelength, the SH signal is expected to decrease as $|\phi_2+\varphi''(\omega)|^{-1}$ for large positive and negative values of ϕ_2 (i.e. such that $|\phi_2| \gg \max(|\varphi''(\omega)|)$). It follows from (5) that it is theoretically possible to extract analytically $\varphi''(\omega)$ from only two measurements. Indeed, let $\phi_2^{\min}$ and $\phi_2^{\max}$ be two second order coefficients of opposite signs such that $\phi_2^{\min} \ll -|\varphi''(\omega)|$ and $\phi_2^{\max} \gg |\varphi''(\omega)|$ for all ω, and one then gets:

$$I(\omega) \propto \sqrt{\frac{I_{\min}(2\omega)\times I_{\max}(2\omega)}{I_{\min}(2\omega)+I_{\max}(2\omega)}(\phi_2^{\max}-\phi_2^{\min})} \qquad \text{and} \qquad \varphi''(\omega)=\frac{I_{\min}(2\omega)\phi_2^{\min}+I_{\max}(2\omega)\phi_2^{\max}}{I_{\min}(2\omega)+I_{\max}(2\omega)}, \tag{6}$$

where $I_{\min}(2\omega)=I_{\mathrm{SHG}}(\phi_2^{\min},2\omega)$ and $I_{\max}(2\omega)=I_{\mathrm{SHG}}(\phi_2^{\max},2\omega)$. In other words, for a given angular frequency, the local chirp $\varphi''(\omega)$ is the arithmetic mean of $\phi_2^{\min}$ and $\phi_2^{\max}$ weighted by $I_{\min}(2\omega)$ and $I_{\max}(2\omega)$. By integrating $\varphi''(\omega)$ twice, the spectral phase $\varphi(\omega)$ can be unambiguously retrieved up to a linear phase (the absolute group delay and absolute phase are not measurable in the slow varying envelope approximation). In principle, the input spectrum can also be retrieved by this method if the second harmonic spectra are acquired with a sufficiently high dynamic range (the root square operation performed on the SH spectra tends to amplify the noise). As a result, both the spectral amplitude and phase can be unambiguously measured if at least two far-field SH spectra are acquired (formulas similar to Eq. (6) can be derived for chirp coefficients of the same sign). To the best of our knowledge, equation (6) is the first mathematical proof of the bijective character of the chirp-scan technique.

In the special case of $\phi_2^{\max}=|\phi_2|=-\phi_2^{\min}$, the relations (6) can be simplified:

$$I(\omega) \propto \sqrt{2|\phi_2|\frac{I_{\min}(2\omega)\times I_{\max}(2\omega)}{I_{\min}(2\omega)+I_{\max}(2\omega)}} \text{ and } \varphi''(\omega)=|\phi_2|\frac{I_{\max}(2\omega)-I_{\min}(2\omega)}{I_{\min}(2\omega)+I_{\max}(2\omega)}. \tag{7}$$

Application of this method, referred to as Chirp Reversal Technique (CRT) in this paper, is experimentally demonstrated in section 3.2.

From a mathematical point of view the far-field regime is reached when $\varphi''(\omega)/\phi_2 \ll 1$ for all angular frequencies. Although some complex mathematical condition may be established [21], a empirical rule is $|\phi_2| > 4\sigma_t\sigma_\omega\tau_0^2$ where τ_0 is the pulse duration of the Fourier-Transform-limited pulse and $\sigma_t\sigma_\omega$ is the expected time-bandwidth product of the input pulses, expressed as the product of the temporal and spectral standard deviations.

2. Chirp-scan maps: examples and properties

In this section we briefly review some properties of the chirp-scan maps and describe the characteristic chirp-scan maps associated with frequently encountered spectral phase shapes. $I_{\mathrm{SHG}}(2\omega,\phi_2)$ is obtained by scanning ϕ_2 from $\phi_{2,min}$ to $\phi_{2,max}$ and acquiring N second harmonic spectra. $\phi_{2,min}$ and $\phi_{2,max}$ are chosen to both encompass the SH maxima and extend to the far-field regime.

2.1. Examples

For a perfectly flat spectral phase (i.e. for Fourier-transform limited pulses or $\varphi''(\omega)=0$) a typical chirp-scan map is shown in Fig. 1(a): for all wavelengths the SH signal is maximum at $\phi_2=0$ and decreases symmetrically with respect to the maximum (at $\phi_2=0$). For a Gaussian fundamental spectrum the shape of the SH spectra is also Gaussian for all applied ϕ_2 values and the SH signal decreases as $\left[1+\left(\phi_2\Delta\omega^2/4\ln(2)\right)^2\right]^{-1/2}$ where $\Delta\omega$ is the FWHM spectral

#195491 - $15.00 USD Received 8 Aug 2013; revised 26 Sep 2013; accepted 26 Sep 2013; published 10 Oct 2013

width of the input pulse. For all angular frequencies, the SH drops by a factor of 2 for $|\phi_2| = 8\sqrt{3}\ln 2/\Delta\omega^2 \simeq 1.26\tau_0^2$ and then decays as $1/|\phi_2|$.

For a chirped pulse ($\varphi''(\omega) = \varphi''(\omega_0)$, Fig. 1(b)), the maxima are simply shifted toward the ϕ_2 that compensates the chirp of the input pulse (i.e. to $\phi_2 = -\varphi''(\omega_0)$).

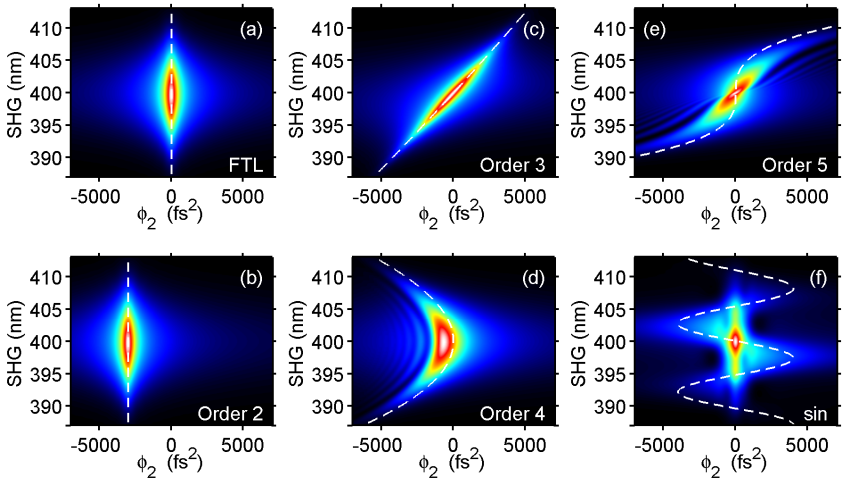

Fig. 1. Chirp scan maps for basic cases of Gaussian shape spectra centered around $\lambda =$ 800 nm with $\Delta\lambda =$30 nm FWHM. The initial spectral phase coefficient of the pulse is set to be (a) zero, (b) 3000 fs^2, (c) 70000 fs^3, (d) 2.10^6 fs^4, (e) 2.10^8 fs^5 and (f) $0.5\times$ sin(100 fs$\times(\omega-\omega_0)$). The overlay white dashed line corresponds to $-\varphi''(\omega)$.

For a third order phase dispersion (Fig. 1(c)), the signal is sheared and the maxima of $I_{\mathrm{SHG}}(2\omega,\phi_2)$ are aligned along the white dashed line revealing $\varphi''(\omega)$. As stated by [7], the maximum SH signal for a given angular frequency 2ω is reached when $\phi_2 = -\varphi''(\omega)$ (stationary phase approximation, see section 1.1). For the third order phase, the second order phase is a linear function of ω and the SH maxima are located at $\phi_2 = -\varphi^{(3)}(\omega_0)(\omega-\omega_0)$.

For a fourth order input phase (Fig. 1(d)), a similar behavior could be expected: the loci of the maxima are expected to follow the parabola $\phi_2 = -\varphi^{(3)}(\omega_0)(\omega-\omega_0) - \varphi^{(4)}(\omega_0)(\omega-\omega_0)^2/2$. The stationary phase approximation is however not exact and the ϕ_2 value for which $I_{\mathrm{SHG}}(\phi_2,2\omega)$ is maximized is not exactly on this parabola.

For a fifth order phase (Fig. 1(e)), the discrepancy is even stronger even if the "S" shaped (cubic dependence of the optimal ϕ_2 on 2ω) can still be recognized.

For a sinusoidal phase (Fig. 1(e)), the figure becomes even more complex and the local maxima are not located at $-\varphi''(\omega)$. Here the maxima are all aligned at $\phi_2 = 0$. In such a case, the stationary phase approximation completely fails. Large parts of the spectrum indeed contribute to the SH signal owing to the broadband intrapulse frequency mixing. The approximation $\phi_{2,max} \simeq -\varphi''(\omega)$ nevertheless holds in some specific cases: when a very small portion of the spectrum contributes to the signal at 2ω (spectral edges for example), spectral phase of large amplitude with slow variations (like in [7]) with a regular spectrum. At the same time, the far-field pattern does follow the expected tendency: on Fig. 1(e) the blue shade indeed follows the white dashed line.

To get an intuitive representation of the chirp-scan maps, we simulate a more dense variety of amplitudes and spectral phases in the attached video (cf. Fig. 2).

#195491 - $15.00 USD Received 8 Aug 2013; revised 26 Sep 2013; accepted 26 Sep 2013; published 10 Oct 2013

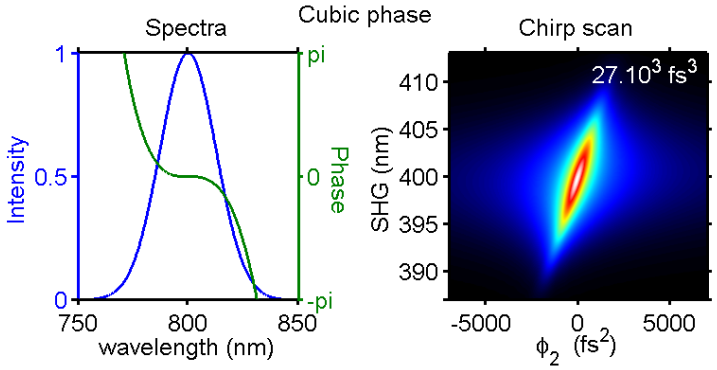

Fig. 2. Snapshot of the video (Media1) showing some typical chirp-scan maps as a function of the spectral amplitude and/or phase distortions. The spectral components (— intensity and — phase) are plotted on the left side while the map is on the right side.

2.2. *Symmetry*

Unlike SH-FROG maps, chirp-scan maps are generally not symmetric with respect to the scanned variable. In fact, it can be shown that the only case for which chirp-scan maps are symmetric with respect to the ϕ_2 axis is when $\varphi''(\omega)$ is constant i.e. for pure quadratic spectral phases. Such feature is extremely practical, since any departure from a perfect "left-right" symmetry indicates the presence of some higher-order spectral phase. From equation (2) one can also deduce that if the spectrum is symmetric with respect to the carrier frequency ω_0 then then an even spectral phase leads to an axial symmetry with respect to $\omega = 2\omega_0$ whereas anti-symmetric spectral phases lead to centro-symmetric diagrams (Fig. 1(c), (e) and (f)).

2.3. *Marginals*

Similarly to the SH-FROG maps, the marginals of chirp-maps contain information of interest. First, the integral of $I_{\mathrm{SHG}}(2\omega,\phi_2)$ along ω is expected to decrease as $1/|\phi_2|$ in the far-field approximation. This hyperbolic decay can be deduced from Eq. (5) and can be used to check if the far-field regime is reached. Secondly, the integral of $I_{\mathrm{SHG}}(2\omega,\phi_2)$ along ϕ_2 is independent of $\varphi(\omega)$ for a given scanning range and a given fundamental spectrum $I(\omega)$, provided that the far-field is reached on the edges of the scan. Equation (2) can indeed be rewritten as:

$$I_{\mathrm{SHG}}(2\omega,\phi_2) \propto \iint_{\mathbb{R}^2} E(\omega-\Omega)E(\omega+\Omega)E^*(\omega-\Omega')E^*(\omega+\Omega')e^{i\phi_2\left(\Omega^2-\Omega'^2\right)}d\Omega d\Omega'. \quad (8)$$

The integration over ϕ_2 with the change of variables $\Omega = (u+v)/2$ and $\Omega' = (u-v)/2$ then leads to:

$$\iiint_{\mathbb{R}^2} E\left(\omega-\frac{u+v}{2}\right)E\left(\omega+\frac{u+v}{2}\right)E^*\left(\omega-\frac{u-v}{2}\right)E^*\left(\omega+\frac{u-v}{2}\right)e^{i\phi_2 uv}du\,dv\,d\phi_2, \quad (9)$$

and finally:

$$\int I_{\mathrm{SHG}}(2\omega,\phi_2)d\phi_2 \propto \Delta\varphi_2 \iint_{\mathbb{R}^2} f(u,v)\mathrm{sinc}\left(\frac{\Delta\varphi_2 uv}{2}\right)e^{i\langle\varphi_2\rangle uv}\,du\,dv, \quad (10)$$

where $f(u,v)$ is a complex-valued function, $\Delta\varphi_2 = \phi_{2,max} - \phi_{2,min}$ and $\langle\varphi_2\rangle = (\phi_{2,max} + \phi_{2,min})/2$. Since the spectral support of the fundamental spectrum is experimentally bounded,

#195491 - $15.00 USD Received 8 Aug 2013; revised 26 Sep 2013; accepted 26 Sep 2013; published 10 Oct 2013

the integral limits are also bounded and the sinc $(\Delta\varphi_2 uv/2)$ term behaves as a sampling function (Dirac function) if $\Delta\varphi_2$ is large enough. More precisely, this condition is $\Delta\varphi_2\Delta\omega^2 \gg \pi$ and corresponds to the far-field approximation. As a result, the integral becomes, to the first order, independent of the spectral phase:

$$\int I_{\mathrm{SHG}}(2\omega,\phi_2)d\phi_2 \simeq \alpha\Delta\varphi_2 f(0,0) = \alpha\Delta\varphi_2 I(\omega)^2, \tag{11}$$

where α is a constant coefficient depending on $\Delta\varphi_2$.

3. Experimental demonstration

3.1. Experimental setup

We use as test pulses the output of a Ti:Sapphire chirped-pulse amplifier delivering 2 mJ pulses at 5 kHz (Dual Legend Elite USX, Coherent). The spectral width of the compressed pulses is $\Delta\lambda \approx 50$ nm FWHM centered at $\lambda_0 = 800$ nm which supports sub-25 fs pulses. The experimental setup consists of a beam sampling plate, an acousto-optic programmable dispersive filter (AOPDF [22]), a 20 μm-tick β-barium borate (BBO) crystal cut for a type I second harmonic generation at 800 nm ($\theta = 29^\circ$), a coloured filter (BG37, Schott) to isolate the SH signal, a focusing lens and a high-resolution spectrometer covering 350-450 nm with a 0.1 nm resolution (AvaSpec2048, Avantes, with a 10 μm input slit). The spectral response of both the spectrometer and the colored filter were calibrated with a blackbody source. The AOPDF is a 25 mm HR-cut TeO_2 crystal (HR800, Fastlite) and is used simultaneously to compensate for the dispersion of the AOPDF itself and add the ramp of quadratic phases required for the chirp-scan measurements and, optionally, compensate the measured spectral phase. After self-compensation the AOPDF was able to add quadratic phases with chirp coefficients ranging from -9000 fs^2 to +9000 fs^2 with a precision better than 1%. Such a span correspond to a pulse broadening is up to about 50 times the FTL pulse duration. Given the thickness of the BBO crystal the finite phase-matching bandwidth does not distort the SH spectrum by more than a few percents at the edges of the SH spectrum (the beam is not focused on the BBO crystal). Pulse durations as given at FWHM with a precision of ± 0.5 fs limited by the shot-to-shot fluctuations.

3.2. Chirp-reversal technique

To test and demonstrate the chirp-reversal technique (CRT) introduced in subsection 1.4, we first use the AOPDF to add sequentially -5000 fs^2 and +5000 fs^2. The corresponding SH spectra are shown in Fig. 3(a). The reconstructed spectra and the second derivative of the spectral phase are displayed in Figs. 3(b) and 3(c) (blue solid curves) and are compared to the spectrum and phase retrieved by the 2D-fit described in the sub-section 3.3. The noise level on the retrieved spectrum is intrinsic to the technique since any noise on the measured SH spectra (or any defect of the phase applied by the AOPDF) will be directly transferred on the retrieved spectrum. To avoid numerical artifacts the SH spectra were smoothed and apodized before applying formula 7. The analytic reconstruction is still very close to the real spectrum. The retrieved spectral phase is complex and is composed of high-order polynomial phase and oscillating features. Although this phase structure was confirmed by further experiments, its physical origin was not explored.

This experiment demonstrates that a chirp-scan reduced to only 2 acquisitions can already provide a decent measure of the spectral amplitude and phase. However, as already mentioned, the experimental data do not contain redundant information and potential measurements artifacts cannot be discarded. To overcome this problem, some additional data are required. The advantages of a full chirp-scan are manifold: noise is reduced in the retrieved data, the interpretation is far more intuitive, the conditions of far-field do not have to be fulfilled. On the other

#195491 - $15.00 USD Received 8 Aug 2013; revised 26 Sep 2013; accepted 26 Sep 2013; published 10 Oct 2013

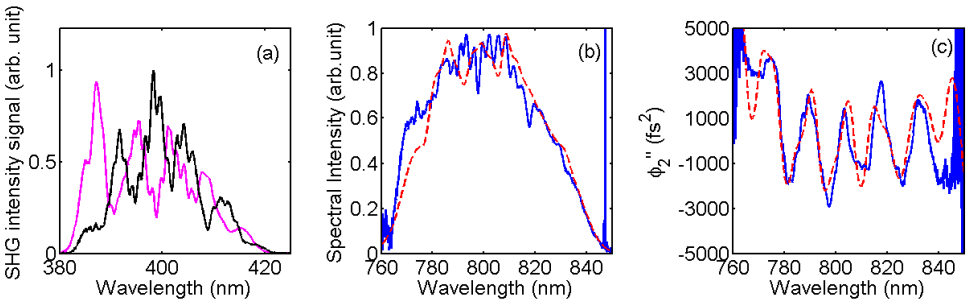

Fig. 3. *(a)* SH spectra recorded at +5000 fs^2(— in black) and -5000 fs^2(— in magenta). The reconstructed spectral intensity *(b)* and the second derivative of the phase *(c)* shown in blue solid line for the CRT reconstruction technique and in red dashed line for our 2D-fit technique described in the following.

hand, an iterative algorithm is required in order to reconstruct the test pulses. The two techniques are, in fact, complementary since a chirp-scan usually contains data compatible with the CRT and the iterative algorithm requires relevant initial conditions. In the following sections we combine both retrieval methods (analytical and blind reconstructions).

3.3. Iterative algorithm

In this subsection we use an optimization algorithm to reconstruct the spectral amplitude and phase from a full chirp-scan map (the number N of SH spectra recorded is typically 64). The fitting procedure is based on a standard Levenberg-Marquardt least-square fit procedure. Unlike [12], we assume that $R(2\omega)$ is known (i.e. calibrated spectrometer, perfect phase-matching) and we reconstruct simultaneously **both** the spectral amplitude **and** the spectral phase. Such an assumption can be experimentally justified for pulse durations longer than $\simeq$10-15 fs. The main advantage of this approach is to avoid an independent measurement of the spectrum and potential artifacts such as beam inhomogeneities or amplified spontaneous emission do not come into account. Our procedure proceeds all the data in a single loop. The fit parameters are directly the sampled spectral amplitude and the second derivative of the spectral phase ($|E(\omega_i)|$ and $\varphi''(\omega_i)$ for i ranging from 1 to N_s). Working with the second derivative (i.e. local chirp) rather than with the phase directly is warranted by the fact that, in the slowly varying envelop approximation, the SH signal is insensitive to the absolute and linear phase. We use the result of the CRT algorithm as initial conditions to start the fit with reasonable initial conditions for the amplitude and phase parameters. Using this strategy, the convergence of the algorithm is very stable and we found numerically that it always converges towards the same solution. With $N \simeq N_s \simeq 64$ and about 200-300 spectral points a typical convergence time is about 10 s with a standard laptop computer.

3.4. Example 1: complex chirped pulse

To validate our technique we record the chirp-scan map, retrieve the spectrum and spectral phase by combining CRT and the 2D-fit and then correct the reconstructed spectral phase with the AOPDF by adding the opposite of the measured spectral phase. For this experiment we intentionally misalign the grating compressor of our laser system. Figure 4 presents the experimental chirp-scan map (Fig. 4(a)) and the reconstructed map (Fig. 4(d)). The same data are shown after a single phase feedback loop (Figs. 4(b) and 4(e)). After feedback the trace is "focused" at $\phi_2 = 0$ and is almost symmetric with respect to it. As mentioned in subsection 2.2 this

#195491 - $15.00 USD Received 8 Aug 2013; revised 26 Sep 2013; accepted 26 Sep 2013; published 10 Oct 2013

is a strong indication of an FTL pulse. The spectrum, phase and time profile before and after feedback are compared in Figs. 4(c) and 4(f). The higher order spectral phase is corrected and the pulse satellites are efficiently suppressed.

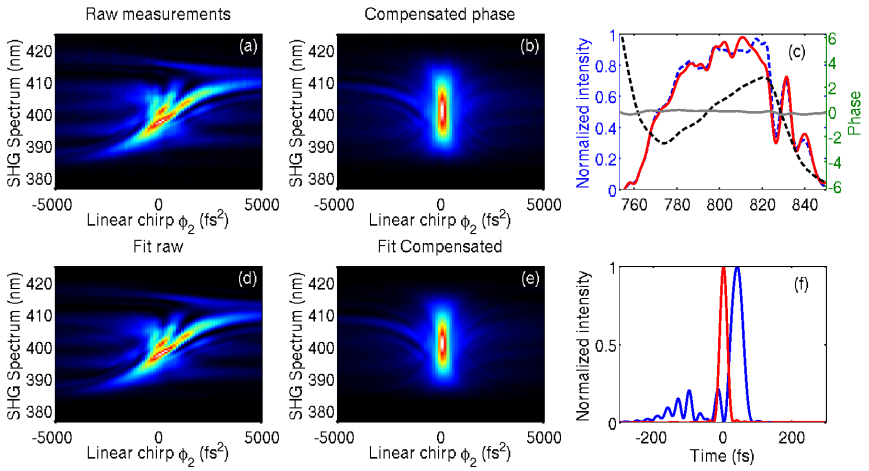

Fig. 4. Measurement and feedback experiment. *(a)* and *(d)* experimental chirp-scan map the reconstructed map before phase feedback. *(b)* and *(e)* same as *(a)* and *(d)* but after feedback. *(c)* and *(f)* the retrieved spectrum, spectral phase, and temporal intensity before (- - - in blue (intensity) and - - - black (phase)) and after (— in red (intensity) and — gray (phase)) correction. The retrieved spectral phase before and after the phase feedback are respectively displayed in solid gray and dashed black *(c)*.

3.5. Example 2: near-FTL pulse

Since the compensation of a strong spectral phase doesn't necessary demonstrate the precision of the measurement, we perform the same experiment when the grating compressor re-aligned. The experimental map (Fig. 5(a)) is almost symmetric and well centered but a single phase feedback can still improve these features (Fig. 5(b)). The time profiles before and after feedback loop are shown in Fig. 5(f). The FWHM pulse durations before and after the measurement-correction loop are equal to 25.5 fs and 23.8 fs. However, the pulse contrast was increased from 10 dB to more than 20 dB. Despite the small values of the initial spectral phase, the chirp-scan map exhibits significant variations. In this experiment, the pulse contrast after the phase correction was limited by the modulations on the spectrum and by the spectral clippings at 760 nm and 850 nm.

3.6. Calibration of the ϕ_2 axis

In [12] it is briefly mentioned that the dispersion can be retrieved from the experimental maps. In this section we detail the condition for which the ϕ_2 values can be accurately retrieved by the fit algorithm. A precise knowledge of the chirp values ϕ_2 is indeed not required and the measurement is somehow "self-calibrated". This striking property can be intuitively explained by the fact that, as in the case of the FROG, the two coordinates (wavelength and chirp) are not independent: a trace corresponding to a physical signal has to fulfill some constraints in the frequency-chirp space. For example, the SH signal cannot vanish within tens of fs^2 if the pulse bandwidth is only a few nanometers wide. As a result, if the spectrometer is assumed to be perfectly calibrated, the chirp values ϕ_2 introduced by the AOPDF can be retrieved. In practice,

#195491 - $15.00 USD Received 8 Aug 2013; revised 26 Sep 2013; accepted 26 Sep 2013; published 10 Oct 2013

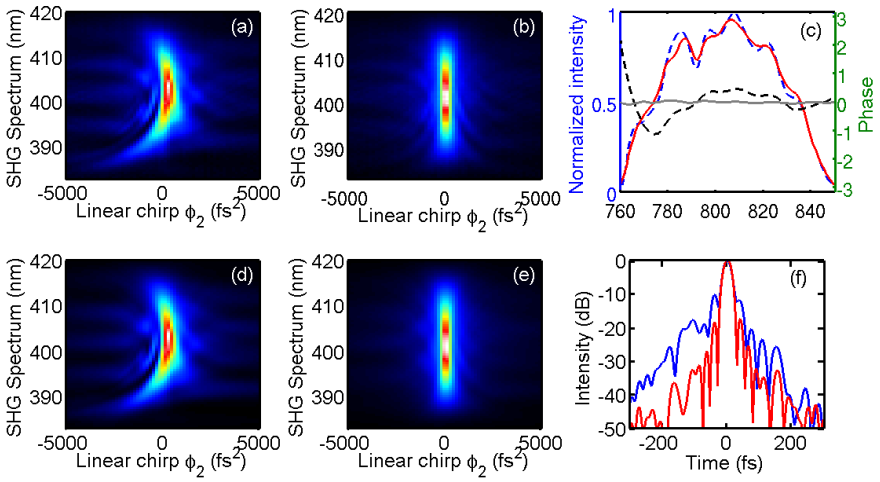

Fig. 5. Same legend as Figure 4.

it is necessary to set at least two ϕ_2 conditions: the global ϕ_2 offset (i.e. the origin of the ϕ_2 axis), the direction of the ϕ_2 axis (otherwise the algorithm might reconstruct $-\varphi''(\omega)$ instead of $+\varphi''(\omega)$). We chose to set $\phi_2 = 0$ when no spectral phase is introduced by the AOPDF.

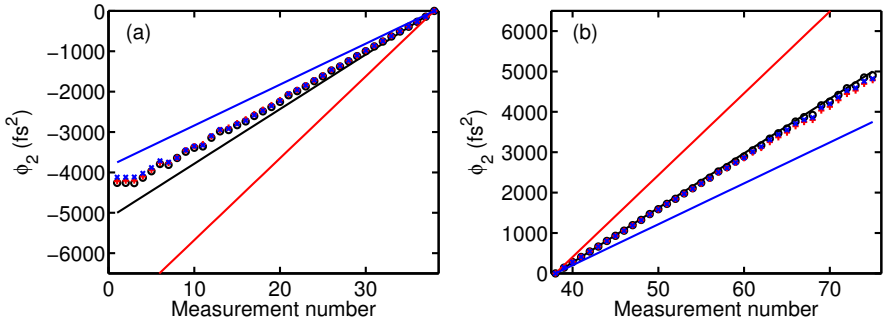

Fig. 6. Robustness of the ϕ_2 axis retrieval. To ease the reading, the negative (a) and positive (b) portions of the ϕ_2 axis are displayed separately. In solid lines are presented the ϕ_2 initial values: expected values from the AOPDF (black), 1.5$\times$ the expected values (red) and 0.75$\times$ the expected values (blue). The symbols represent the final (i.e. retrieved) values by the least-square algorithm (same color code than for the initial values).

To test the robustness of the ϕ_2 reconstruction, we try to reconstruct the experimental map displayed in Fig. 6 with different set of initial conditions for ϕ_2. The initial conditions are obtained by multiplying the expected ϕ_2 values by 1 (black solid line), 1.5 (red solid line) and 0.75 (blue solid line). As done previously, the initial guess of the spectral amplitude and spectral phase are determined with the CRT method. Independently of the initial conditions, the ϕ_2 values retrieved by the algorithm are almost identical (blue, red and black dots are superposed on Fig. 6) and almost match the expected values (black solid line). A small discrepancy can however be noticed for large negative ϕ_2 values. This discrepancy may originate from a small calibration error of the AOPDF and is stronger for negative value because of the dispersion bias

#195491 - $15.00 USD Received 8 Aug 2013; revised 26 Sep 2013; accepted 26 Sep 2013; published 10 Oct 2013

(the AOPDF also compensates for its own dispersion of about -13000fs^2).

4. Comparison with reference techniques

In the same spirit as [14] we cross-check our measurements with reference devices. In this section we compare chirp-scan with a home-built b-FROG [16] and with a commercial SRSI [17, 23] device (Wizzler800, Fastlite). The experimental protocol is the following: the pulses are characterized by chirp-scan, the retrieved spectral phase is compensated by the AOPDF and the pulses are characterized by b-FROG or by SRSI. These techniques were selected for the following reasons: b-FROG measurements can be implemented with exactly the same optical setup (no additional optics), SRSI is based on a radically different principle and the dynamic range of SRSI can reach 45dB [24].

4.1. Comparison with b-FROG

For the b-FROG measurements, the AOPDF produces two pulses replicas of the input pulse and scans the interpulse delay. The spectrometer records the SH spectrum and the b-FROG map is processed by an iterative algorithm. To avoid rescaling and sampling issues, we chose to use the same 2D least-square fitting procedure to extract the spectral amplitude and phase. The results of the reconstruction are shown in Fig. 7. The two measurements agree satisfactorily.

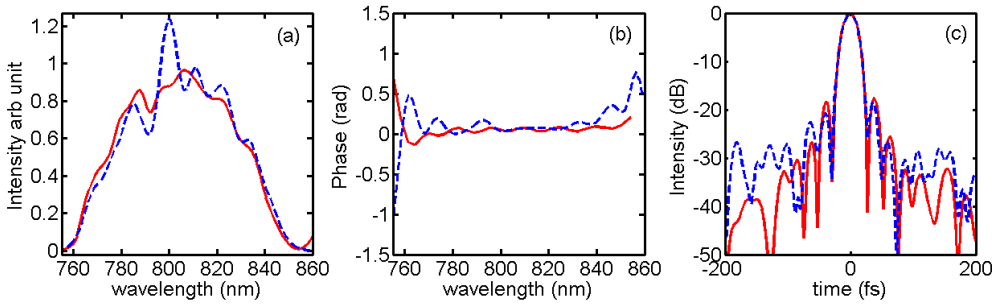

Fig. 7. Comparison of the spectral (*a*) intensity and (*b*) phase and (*c*) the temporal profile reconstructed by the b-FROG (blue dashed line) and the chirp-scan (red solid line).

4.2. Comparison with SRSI

We now compare chirp-scan with SRSI and evaluate the accuracy of the pulse compression. Figure 8 shows an excellent agreement on the spectral phase. Some minor discrepancy in the retrieved spectrum can be noticed. The reconstructed temporal profiles match well down to -25 dB (3.10^{-3}) with respect to the maximum intensity. The time delays of the pre- or post-pulses also match at -30 dB. The discrepancies are believed to be related to the differences in the measured points of the spatial profile. As the fundamental spectrum wasn't perfectly homogeneous over the spatial profile it is possible that the two devices sampled different parts of the input beam.

5. Dispersion-scan with a grating compressor

A major difference between this work and the references [12–14] is that an AOPDF pulse shaper was used to scan the phase parameter. Ideally, such a technique would gain in simplicity if it could be implemented with regular passive optics. Miranda *et al.* [13] showed that a prism pair could be used. However, this solution is not very convenient for narrowband pulses (i.e. $<$50 nm

#195491 - $15.00 USD Received 8 Aug 2013; revised 26 Sep 2013; accepted 26 Sep 2013; published 10 Oct 2013

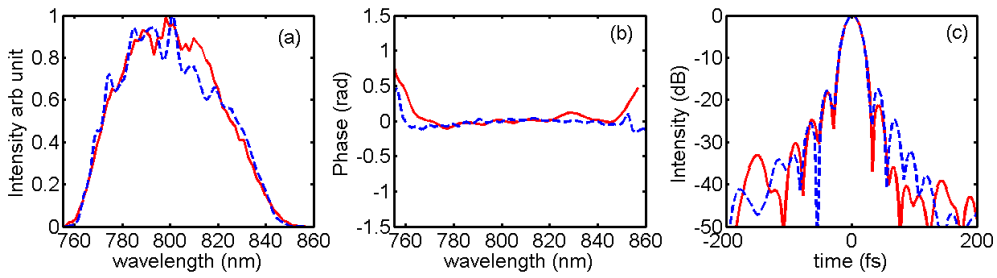

Fig. 8. Spectral and temporal characteristic of the pulse measured by SRSI [23, 24] (blue dashed line) and chirp-scan (red solid line).

FWHM at 800nm): the dispersion of a prism pair is indeed rather low and large propagation distances might be required. In this section we show that, at the cost of a dispersion calibration step, the compressor of the laser system itself can be used directly for the scan.

To measure the third order and higher order dispersion introduced by the grating compressor, we first optimize the pulse duration by chirp-scan and record a reference chirp-scan map. The distance between the gratings is then gradually varied and consecutive chirp-scan maps are recorded. Typical measurements are shown in Fig. 9. As can be seen at first glance, changing the gratings distance changes both the second order dispersion (shifted traces) and the third order dispersion (sheared traces) of the pulses. To extract the second, third and fourth order

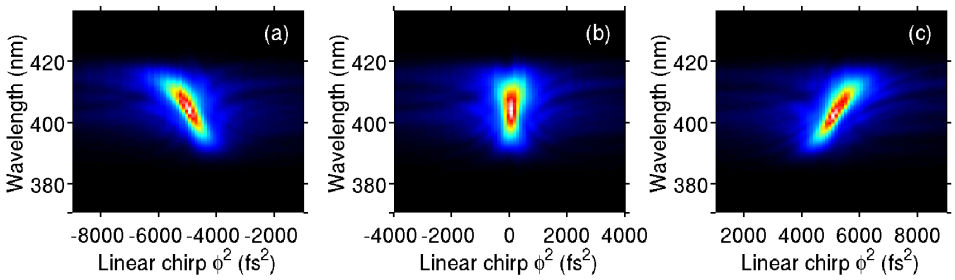

Fig. 9. d-scan measurements realized when the diffraction grating is before (*a*), at (*b*) and after (*c*) the compression optimization.

dispersion coefficients of the compressor as a function of the grating separation, the spectral phase is retrieved for each grating position and the reconstructed phase is fitted by a fourth order polynomial. The resulting third and fourth orders of dispersion are shown in Fig. 10 as functions of the second order coefficient.

Figure 10(a) shows a linear dependence of the third order dispersion with chirp. The fourth order dispersion was found almost constant (Fig. 10(b)) within the experimental error. To the first order, the ratio of the third order dispersion coefficient ϕ_3 to ϕ_2 is almost constant and given by:

$$\frac{\phi_3}{\phi_2} = (-2.067 \pm 0.026)\ \text{fs}. \tag{12}$$

The theoretical value (groove density of 1500 g/mm and incidence angle of 50°) is -2.09 fs at 800 nm and it agrees well with the experimental value. Calculations also give a ϕ_4 to ϕ_2 ratio of 7.0 fs^2 at 800 nm, which is also in agreement with the measurements. Once the compressor is calibrated, the third order dispersion is taken into account by the chirp-scan algorithm. As

#195491 - $15.00 USD Received 8 Aug 2013; revised 26 Sep 2013; accepted 26 Sep 2013; published 10 Oct 2013

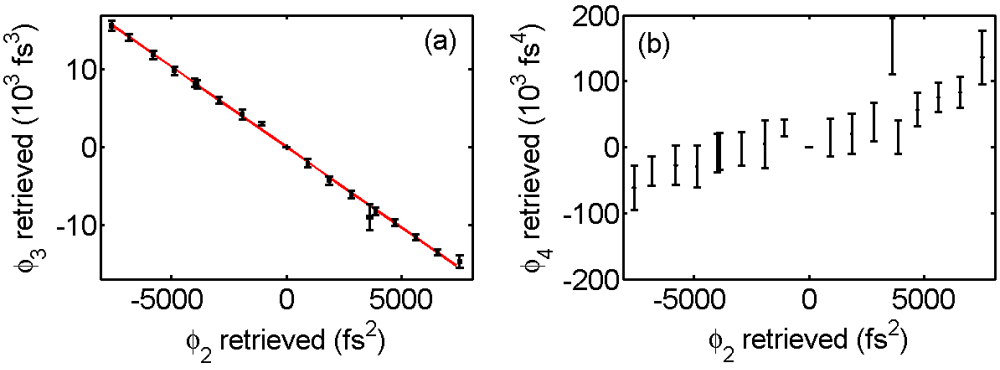

Fig. 10. Correlation of the order 2 with (*a*) the order 3 and (*b*) the order 4 of the phase dispersion induced by the CPA compressor. Error-bars are displayed vertically and horizontally. A linear fit (solid line) has been realized for (*a*).

we previously demonstrated (Figure 6) it is not necessary to accurately know the real value of the applied chirp, it is possible to simply scan the gratings separation distance without even measuring the actual displacements.

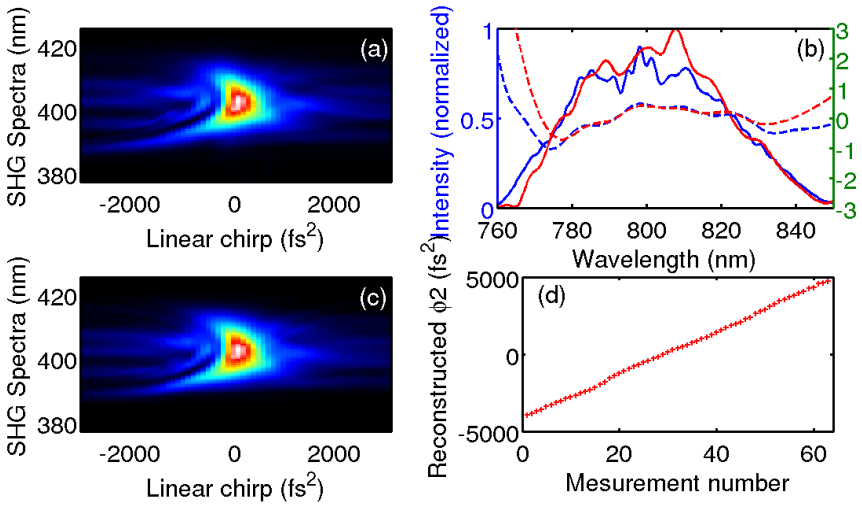

Fig. 11. Grating d-scan acquisition "on-the-fly" (*a*) and its respective fit (*c*). The spectral intensity (solid line) and phase (dash line) are presented in (*b*) for the present measurement (red) and a reference measurement realized with a standard d-scan (blue). The retrieved linear chirp ϕ_2 that we have introduce with the grating is shown in (*d*) and the third order is given by the equation (12).

The implementation of the third order correction in the 2D-fit algorithm is straightforward: an additional term in included in the calculations. In our case, as we do not control the absolute position of the grating with the translational stage we reconstruct at once the amplitude, the phase and the added dispersion. Experimentally, one spectra was recorded every 50 ms "on-the-fly" while continuously scanning the distance between the compression gratings with a manual linear translation stage. The results are shown in Fig. 11. These measurements are then

#195491 - $15.00 USD Received 8 Aug 2013; revised 26 Sep 2013; accepted 26 Sep 2013; published 10 Oct 2013

compared to an AOPDF-based chirp-scan. The reconstruction is as good as with the AOPDF and the algorithm stability is not affected by the introduction of the ϕ_3 correction. It is worth noting that the retrieved chirp values are not perfectly regular as shown in Fig. 12(d) (the translation speed wasn't perfectly constant due to the manual operation), which shows that, as stated before, the φ_2 values can be accurately retrieved.

6. Conclusions

Chirp-scan, and more generally dispersion-scan, is a powerful technique to characterize short pulses. Varying chirp instead of more complex phase functions provides an intuitive access to the spectral phase content and simple criteria to assess the pulse compression quality (symmetry). We showed that both the spectrum and the spectral phase can be retrieved by chirp-scan either analytically or by running a simple iterative algorithm and that the minimal number of measurements is 2. We also showed that this technique is free from non-trivial ambiguities if the chirp range is large enough and that this technique is, in a sens, self-calibrated. 25fs pulses delivered by amplified Ti:Sapphire system were characterized by chirp-scan and the measurements were compared to the measurements provided by two reference techniques. The results nicely agree and the dynamic range of the chirp-scan measurements could be assessed to at least two orders of magnitude.

We believe that most of these features and characteristics would hold for a general d-scan (not demonstrated here). As an example, we described how a calibrated grating compressor could be used to perform a simple d-scan measurement. Since any available dispersive setup (pulse shaper, grating compressor, prism compressor, glass wedges and chirped mirrors...) could be virtually used, the d-scan technique could easily be implemented in most existing setups to characterize pulses with durations ranging for a few ps to few optical cycles.

Acknowledgment

The ANR Muse (ANR-10-BLAN-0428-01) is gratefully acknowledged.

#195491 - $15.00 USD Received 8 Aug 2013; revised 26 Sep 2013; accepted 26 Sep 2013; published 10 Oct 2013